Nano Today 48 (2023) 101741

Contents lists available at ScienceDirect

Nano Today

journal homepage: www.elsevier.com/locate/nanotoday

Clusters of polymersomes and Janus nanoparticles hierarchically self-organized and controlled by DNA hybridization

Voichita Mihali [a,b], Michal Skowicki [a,b], Daniel Messmer [a], Cornelia G. Palivan [a,b,*]

[a] Department of Chemistry, University of Basel, Mattenstrasse 24a, 4058 Basel, Switzerland
[b] NCCR Molecular Systems Engineering, Mattenstrasse 24a, 4058 Basel, Switzerland

ARTICLE INFO

Article history:
Received 31 August 2022
Received in revised form 13 November 2022
Accepted 23 December 2022
Available online 3 January 2023

Keywords:
Janus nanoparticles
Polymersomes
Self-organization
Hybrid materials
Encapsulation of molecules

ABSTRACT

The combination of "hard", structurally well-defined particles with "soft", functional compartments bears great potential to produce structurally intricate hybrid nanomaterials that promote a multitude of applications that require multimodal agents and that permit the production of molecular factories. However, the co-assembly of "hard" and "soft" components in a programmable and directional manner is challenging due to the strongly differing mechanical properties of such disparate entities. Here, a versatile strategy to generate clusters by the directional and controlled self-organization of "hard" Janus nanoparticles (JNPs) with "soft" polymersomes is described. The hybridization of complementary ssDNA strands bound to the components drives cluster formation, while the asymmetry of the JNPs governs the directionality of the self-organization. Various factors have been explored to simultaneously preserve the integrity of the polymersomes and program the cluster formation. Differently loaded polymersomes on each lobe of the JNPs preserved their architecture in the clusters which, were shown to be non-toxic when interacting with cell lines. The architecture of the clusters, as a molecular factory where each component can be separately controlled bears great promise for use in advanced medical applications, including theranostics and correlative imaging.

Introduction

Hierarchical self-organization is a key paradigm in biological systems, creating large, well-defined superstructures from self-assembled subunits, which in turn consist of molecular components. [1,2] This spanning of size scales and the resulting emergent functionality have long inspired researchers from various disciplines. [2–7] Self-organized nanomaterials are consequently investigated for various applications, including optical materials, [8–11] flexible electronics, [12,13] and biomedicine. [14–17] Many biomedical applications such as correlative imaging, [18,19] theranostics, [20,21] or multimodal therapeutic approaches [22,23] require the targeted co-delivery of several, at times incompatible components. The hierarchical assembly of dissimilar components at the nanoscale (nanoparticles, nanotubes, vesicles *etc.*) into integrated systems with the organization as a molecular factory is therefore in high demand, to provide the desired multifunctionality and to control the behavior of the components.

Nanoparticles offer well-defined dimensions and the potential to act as scaffolds for highly precise, directional assembly, but on their own they are often cytotoxic [24] and lack the functionality and responsiveness desired in the biomedical field. The latter properties are key strengths of "soft" nanoassemblies such as micelles and lipid or polymer vesicles, [25–30] which can protect even delicate, biologically active substances. However, the self-organization of soft nanoassemblies is difficult to control, *e.g.* because of aggregation of vesicle clusters beyond the desired size [31] or the fusion of lipid vesicles, which compromises the desired segregation between vesicle contents. [32].

The co-organization of "hard" and "soft" components promises to combine the above advantages while diminishing the respective disadvantages. However, the incorporation of "hard" and "soft" entities into novel nanomaterials presents its own challenges, especially due to the strongly differing mechanical properties of the components. Many approaches have been explored to form hybrid nanoassemblies, especially those resulting in hybrids between organic and inorganic components. [33–35] Many such studies focus on assemblies incorporating inorganic nanoparticles, *e.g.* attached to the surfaces of nanotubes, [36] peptide fibers, [37] and worm-like micelles, [38] or incorporated into micelles [39] and vesicle membranes. [40,41] However, these self-organized superstructures

* Corresponding author at: Department of Chemistry, University of Basel, Mattenstrasse 24a, 4058 Basel, Switzerland.
E-mail address: cornelia.palivan@unibas.ch (C.G. Palivan).

https://doi.org/10.1016/j.nantod.2022.101741

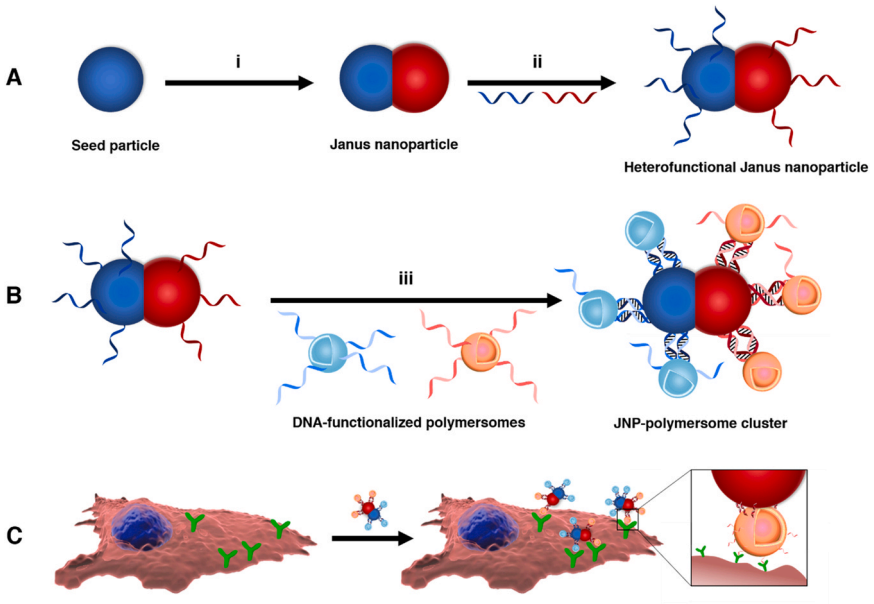

Fig. 1. Schematic representation of JNP-polymersome cluster preparation and cell adhesion. (A) Synthesis of heterobifunctional JNPs by i) seeded emulsion polymerization and ii) chemoselective, directional functionalization with ssDNA; (B) Formation of clusters by iii) combination of ssDNA-functionalized JNPs with complementary ssDNA-functionalized polymersomes; (C) Schematic representation of the interaction of JNP-polymersome clusters with cell membrane receptors.

typically rely on unspecific interactions, and only relatively few examples exist that demonstrate functional assemblies with precisely controlled structures. [42–45] Importantly, a general approach to the production of hybrid "hard/soft" colloidal superstructures, where the components have very dissimilar properties (*e.g.* mechanical stability), to allow for highly modular functionality has not yet been developed.

Here, we aim to fill this gap by introducing a programmable strategy for the directional self-organization of disparate components into hybrid “hard/soft” clusters that promote a controlled and segregated localization of different compounds. We selected polymer-based Janus nanoparticles (JNPs) as a “hard”, asymmetric, colloidal platform. [46–49] The chemically or physically distinct, spatially separated lobes of JNPs [46,50] support directional self-organization, as previously demonstrated for nanoparticle clusters. [51] Polymersomes based on the diblock copolymer PDMS-*b*-PMOXA are used as the “soft” component. They provide a confined space for reactions, [52–54] have a flexible [55–57] but mechanically stable membrane, [58,59] and are non-toxic, [60] which are all key properties for the targeted bio-applications. Additionally, polymersomes have been shown to preserve their integrity in self-organized clusters, maintaining the encapsulation of cargo. [57,61,62] From among the various supramolecular motifs employed to drive self-organization, [63–67] we selected ssDNA strands to link the components. [51,61,62,68,69] ssDNA hybridization advantageously provides a strong, highly specific interaction and an unparalleled extent of programmability [70,71] properties previously leveraged *e.g.* in the production of novel materials such as patterned surfaces [42,72] or nanoparticle superlattices. [73–75] The orthogonally addressable surface functionalities of the JNP lobes [47,49] were selectively modified with ssDNA strands (each lobe with a specific ssDNA sequence, Fig. 1A), whilst polymersomes were functionalized by attaching ssDNA complementary to that on either JNP lobe (Fig. 1B).

Preserving the integrity of each component in the clusters requires a detailed understanding of the self-organization process, as the significant difference in properties (*e.g.,* mechanical stability, accessibility of ssDNA strands) between “hard” JNPs and “soft” polymersomes results in complex interactions. By systematically exploring various parameters of polymersome and cluster preparation, we aimed to achieve rapid and directional self-organization into a molecular factory architecture where each each component can be separately controlled at the nanoscale.

To determine whether the resulting clusters are suitable for bio-applications, such as the encapsulation of functional cargo [76–79] or enzymatic cascade reactions *e.g.* for signaling cascades, [80–82] we loaded the constituent polymersomes with model molecules and tested the clusters’ toxicity and interactions with two cell lines (Fig. 1C). The lack of cytotoxicity and specific interactions with cell receptors are complemented by the unique features of the clusters, including high modularity of formation and the ability to co-encapsulate, yet spatially separate, different active cargos. These hybrid colloidal systems self-organized are predestined in particular for applications that require multimodality and exquisite control, such as correlative imaging, reaction cascades, or theranostics.

Methods

Selective modification of carboxylic acid groups on JNP-II with ssDNA

For the modification of carboxylic acid groups by EDC/sulfo-NHS coupling, **JNP-II** (15 mg) were first dispersed in a mixture containing EDC solution (400 µL, 0.2 M in UPW), sulfo-NHS solution (800 µL, 0.2 M in UPW), and one crystal of DMAP. The resulting suspension was stirred for 2 min, and then a 5′-amino-terminated ssDNA solution (100 µL, 0.2 mM in UPW, *e.g.* **a**) was added to the reaction. The reaction was stirred at room temperature for 24 h, after which the JNP-ssDNA conjugate (*e.g.* **JNP-a**) was isolated by centrifugation and washed sequentially three times with ethanol and UPW, and two times with PBS. The final suspension was stored in 2 mL PBS at 4 °C. See Supporting Information, Table S3, S4, and S5 for characterization by SEM, Zeta potential, and FCS.

Selective modification of azide groups on JNP-II with ssDNA

For modification of azide groups by SPAAC, **JNP-II** (15 mg) were first dispersed in dimethylformamide (0.5 mL), then a solution of 5′-DBCO-terminated ssDNA (100 µL, 0.2 mM in UPW, *e.g.* **c**) was added. The reaction was stirred at room temperature for 24 h. The JNP-

ssDNA conjugate (*e.g.* **JNP-c**) was then isolated by centrifugation, and washed sequentially three times with ethanol and UPW, and two times with PBS. The final suspension was stored at 4 °C in PBS (a final volume of 2 mL). Then, the same procedure was applied for double functionalization of JNPs with ssDNA but in this case **JNP-a** was used as the starting material. See Supporting Information Table S3, S4, and S5 for characterization by SEM, Zeta potential, and FCS.

Conjugation of ssDNA to polymersomes

Polymersome dispersion (200 µL) was mixed with a solution of 5′-DBCO-terminated ssDNA (0.2 mM in UPW, 1.2 equivalents per azide group). The reaction was allowed to proceed overnight at 40 °C with shaking at 300 rpm. The solution was purified by SEC to remove free DNA, then stored at 4 °C in PBS (2 mL total volume). See Supporting Information, Table S6, S7, and S8 for characterization by SLS/DLS and FCS.

Preparation of JNP-polymersome clusters

The concentrations of polymersome and JNP precursors were estimated by NTA (typically $1–5 \times 10^{11}$ particles/mL). In a typical experiment, a volume containing approx. 2×10^9 ssDNA-conjugated Janus nanoparticles was mixed with a volume containing approx. 10×10^9 ssDNA-conjugated polymersomes. The mixture was adjusted to a total volume of 300 µL with PBS, and the self-organization was allowed to proceed overnight at 37 °C with shaking at 300 rpm. Clusters were analysed by TEM imaging, and their composition determined by analysis of 20–25 TEM micrographs of three independent JNP-polymersomes cluster batches.

All information regarding: materials; methods; oligonucleotide sequences; detailed synthesis and characterization of PtBA seed nanoparticles; detailed synthesis and characterization of Janus nanoparticle precursors, Janus nanoparticles, and Janus nanoparticle conjugates; synthesis and characterization of $PDMS_{28}$-*b*-$PMOXA_{10}$-N_3; detailed characterization of polymersomes, polymersome conjugates and Janus nanoparticle-polymersome clusters; characterization of polymersome and Janus nanoparticle conjugates with long ssDNA linkers and the clusters formed thereof; additional details regarding *in vitro* toxicity and cell adhesion studies are reported in the Supporting Information.

Results and discussion

Synthesis of JNPs and selective, asymmetric functionalization with ssDNA

To obtain particles suitable for asymmetric self-organization, JNPs were prepared by seeded emulsion polymerization and phase separation under surfactant-free conditions. The JNPs were then selectively functionalized with ssDNA strands, employing orthogonal conjugation reactions to address the chemically distinct JNP lobes (Fig. 2A, see Supporting Information, Table S1-S2 for all oligonucleotide sequences).

Poly(*tert*-butyl acrylate) (PtBA)-based, cross-linked seed nanoparticles were prepared by mini-emulsion copolymerization of *tert*-butyl acrylate with sodium styrene sulfonate and divinylbenzene. [46] The resulting spherical particles (diameter of 270 ± 1 nm) were used for the seeded emulsion copolymerization of 3-(triethoxysilyl) propyl methacrylate and 3-azidopropyltrimethoxysilane (Fig. S1, Supporting Information). [47,83] The initial temperature-induced phase separation during the polymerization process produced Janus nanoparticles with two clearly separated lobes, their polymer networks interpenetrating only in the boundary region, bearing *tert*-butyl ester and azido groups, respectively (**JNP-I**). The *tert*-butyl ester groups were then hydrolyzed under acidic conditions, resulting in carboxylic acid groups as evidenced by FTIR spectroscopy and zeta-potential measurements. The azide lobe remained unchanged after PtBA hydrolysis (Fig. S2, Table S3, Supporting Information). Hydrolysis afforded **JNP-II** (Fig. 2B), which uniquely bears spatially separated, orthogonally addressable carboxylic acid and azide groups, and represents an anisotropic platform that is suitable for the attachment of a wide range of molecules, using ester or amide bond formation and alkyne/azide cycloaddition reactions.

We leveraged this orthogonality by selectively attaching two distinct ssDNA strands to the lobes. The carboxylic acid-bearing lobe was functionalized with the 5′-amino-terminated ssDNA **a** (Table S1, Supporting Information, for oligonucleotide sequences) *via* the *N*-(3-dimethylaminopropyl)-*N*′-ethylcarbodiimide/*N*-hydroxysulfosuccinimide sodium salt) (EDC/sulfo-NHS) reaction, [84] and resulted in **JNP-a** (Fig. 2C). The azide-functionalized lobe was decorated with the 5′-dibenzocyclooctyne (DBCO)-terminated ssDNA **c** *via* strain-promoted alkyne/azide cycloaddition (SPAAC) [85] to form **JNP-c** (Fig. 2D). Dual functionalization was achieved by functionalizing the second lobe of **JNP-a** with **c** to produce **JNP-ac** (Fig. 2E, Table S3, Supporting Information). ssDNA functionalization neither affected the shape of the particles nor led to aggregation, as evidenced by essentially unchanged scanning electron microscopy (SEM) micrographs (Fig. 2, B-E, Table S3, Supporting Information).

To study the attachment of the ssDNA strands **a** and **c** to the acid and azide lobes of **JNP-II**, respectively, we used fluorescence correlation spectroscopy (FCS), determining the diffusion times and the numbers of fluorescent molecules moving through a confocal volume. The presence of ssDNA strands (**a** and **c**) on the surface of JNPs was confirmed by hybridization with fluorescently labeled complementary ssDNA strands, namely **b**-Cy5, which is complementary to **a**, and **d**-Atto488, which is complementary to **c**. Successful DNA hybridization was indicated by a significant increase in the diffusion times when comparing free **b**-Cy5 (τ_D = 111 ± 9 µs) to its mixture with **JNP-a** (τ_D = 28 ± 4 ms). A similar increase in diffusion time was observed when comparing free **d**-Atto488 (τ_D = 118 ± 11 µs) to its mixture with **JNP-c** (τ_D = 25 ± 6 ms; Fig. 2F, G and Table S4, Supporting Information). In addition, brightness measurements of the tracked fluorophores (counts per molecule, CPM) enabled quantification of the number of ssDNA strands per JNP lobe (see Methods and Table S5, Supporting Information). Averages of 75 ± 18 **a** ssDNA strands were attached to the acid-functional lobe of **JNP-a** and 40 ± 13 **c** ssDNA strands to the azide-functional lobe in **JNP-c**.

To demonstrate the asymmetry of the functionalization, we simultaneously added **b**-Cy5 and **d**-Atto488 to Janus nanoparticles with both lobes functionalized (**JNP-ac**). The resulting dual-fluorescent JNPs were investigated by confocal laser scanning microscopy (CLSM) on an amino-functionalized glass slide. CLSM Z-stack micrographs show a clear separation between the Cy5- and Atto488-labelled lobes of JNPs, and a preferential orientation of the Cy5-labelled lobes toward the slide surface (Fig. 2H). Evidently, the positively charged slide surface interacts electrostatically with the lobe bearing ssDNA **a** (hybridized with **b**-Cy5), which bears negatively charged carboxylate and sulfonate groups, whereas interactions with the hydroxyl and azide groups on the opposite lobe are significantly weaker. The relatively low average density of ssDNA on both JNP lobes (< 1 ssDNA strand per 1000 nm^2, Table S5, Supporting Information) does not completely shield these strong interactions, and results in a specific orientation of labelled **JNP-ac** relative to the slide surface (Fig. 2H).

Preparation of ssDNA-functionalized polymersomes

Polymersomes were prepared by the film rehydration method, using the diblock copolymer poly(dimethylsiloxane)-*block*-poly(2-methyl-2-oxazoline) ($PDMS_{25}$-*b*-$PMOXA_{10}$-OH, M_n = 2850 g mol^{-1}, Đ

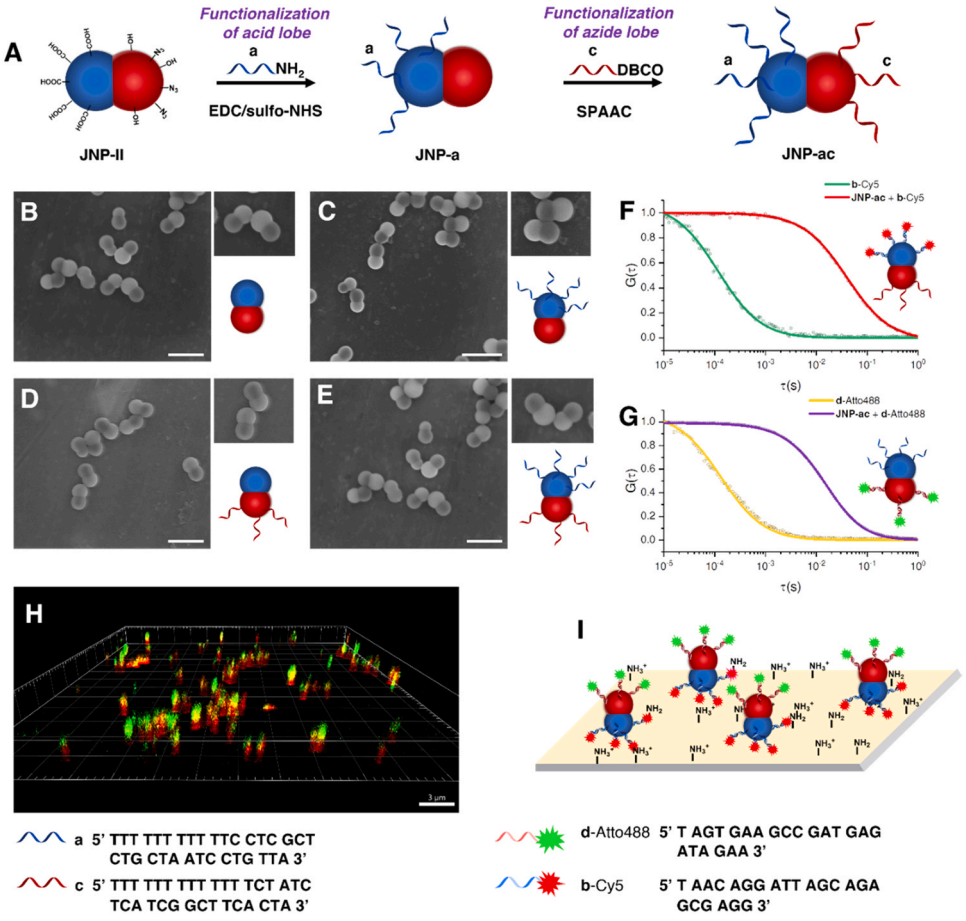

Fig. 2. Asymmetric functionalization of Janus nanoparticles with ssDNA. (A) Schematic representation of orthogonal ssDNA functionalization of JNPs; the lobe bearing carboxylic acid groups (dark blue) is coupled with amino-terminated ssDNA **a** (blue), the azide-bearing lobe (dark red) is coupled with DBCO-terminated ssDNA **c** (red). Schematic representation and SEM micrographs of: (B) **JNP-II**, (C) **JNP-a**, (D) **JNP-c**, and (E) **JNP-ac**. Scale bars = 500 nm. Normalized FCS autocorrelation curves (dots) and fit curves (lines) of: (F) Cy5-labelled ssDNA **b** (**b**-Cy5, 20 nM, red) and **JNP-ac** hybridized with **b**-Cy5 (green); (G) Atto488-labelled ssDNA **d** (**d**-Atto488, 20 nM, yellow) and **JNP-ac** hybridized with **d**-Atto488 (violet). (H) Confocal laser scanning microscopy (CLSM) Z-stack of **JNP-ac** hybridized with both **b**-Cy5 and **d**-Atto488 as observed on an amino-functionalized glass slide; (I) Schematic representation of the orientation of **JNP-ac** after hybridization with ssDNAs **b**-Cy5/**d**-Atto488 when deposited on a positively charged surface.

= 1.49) mixed with a similar, terminally azide-functionalized diblock copolymer ($PDMS_{28}$-*b*-$PMOXA_{10}$-N_3, M_n = 3400 g mol^{-1}, Đ = 1.60; see Section 3 in the Supporting Information and Fig. S3-S6 for details). [61,86] The closely matching PDMS block lengths guarantee a uniform distribution of the azide moieties across the polymersome surface. [87] To examine the influence of functionalization density on polymersome formation, we mixed $PDMS_{25}$-*b*-$PMOXA_{10}$-OH with increasing amounts of $PDMS_{28}$-*b*-$PMOXA_{10}$-N_3 (30 mol%, 50 mol% and 70 mol%). The solutions containing the nano-assemblies were extruded through track-etched polycarbonate membranes with different pore sizes and then analyzed by a combination of dynamic and static light scattering, and by transmission electron microscopy (TEM). The assemblies extruded through 200 nm pore diameter membranes and obtained with 30 mol% or 50 mol% $PDMS_{28}$-*b*-$PMOXA_{10}$-N_3, are referred to as **Pol1** and **Pol2**, respectively, whilst **Pol3** was extruded through a 400 nm pore diameter membrane and comprised 30 mol% $PDMS_{28}$-*b*-$PMOXA_{10}$-N_3. When 70 mol% of $PDMS_{28}$-*b*-$PMOXA_{10}$-N_3 was used in the mixture of copolymers, assemblies with mixed morphology were obtained (Fig. S7, Supporting Information), which were not used.

The hydrodynamic radii (R_h) obtained by dynamic light scattering were: 98 ± 7 nm (**Pol1**), 95 ± 6 nm (**Pol2**), and 194 ± 30 nm (**Pol3**) (Fig. S8, Table S6, Supporting Information). For all nano-assemblies, the ratios between R_h and the radius of gyration (R_g obtained from static light scattering) were close to the theoretical value of 1.0, thus indicating the formation of polymersomes (Table S6, Supporting Information). [88] Zeta-potential values changed slightly as a result of ssDNA attachment (Table S6, Supporting Information). TEM micrographs for **Pol1–3** revealed the typical morphology of collapsed polymersomes (Fig. 3, A-G, and Fig. S9, Supporting Information), whilst Cryo-TEM of **Pol2** indicated the presence of vesicular structures with a membrane thickness of 11.1 ± 0.8 nm (Fig. 3H), in agreement with values reported for PDMS-*b*-PMOXA polymersomes with closely matching block lengths. [61,86].

The azide groups exposed on the polymersomes were functionalized using SPAAC to attach 5′-DBCO-terminated ssDNA **b** (see Table S1, Supporting Information for oligonucleotide sequences). **b** was selected to be complementary to **a**, and ssDNA-conjugated polymersomes **Pol1-b**, **Pol2-b**, and **Pol3-b**, were obtained. Similarly, attachment of 5′-DBCO-terminated ssDNA **d**, which was selected to be complementary to **c**, resulted in **Pol1-d**, **Pol2-d**, and **Pol3-d**. The size and shape of the polymersomes were unaffected by ssDNA conjugation and light scattering indicated that no aggregation occurred (Table S6, Supporting Information). Similar to the characterization of JNPs, we used FCS to confirm and quantify the ssDNA functionalization of polymersomes after hybridizing them with complementary, fluorescently labelled ssDNA strands (**c** labelled with Atto488 or **a** labelled with Cy5, *i.e.,* **c**-Atto488 and **a**-Cy5). The diffusion times of the fluorophore increased for all polymersomes (*e.g.*, from τ_D = 118 ± 17 µs for free **c**-Atto488 to 6.4 ± 2.5 ms for its mixture with **Po** indicating successful hybridization with accessible ssDNA at the surface of the polymersomes (Fig. 3I and Table S7, Fig.

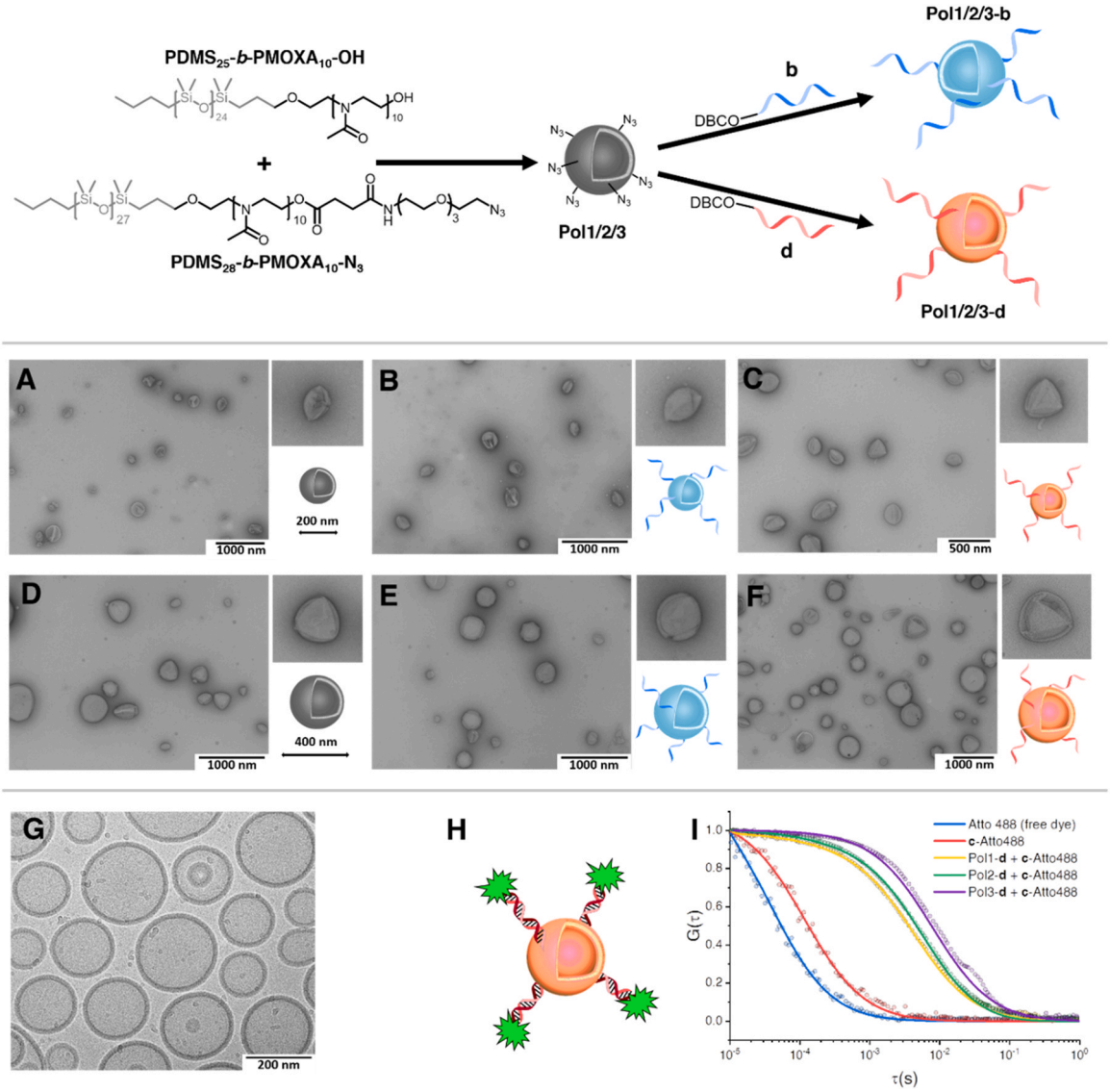

Fig. 3. Formation and ssDNA functionalization of polymersomes. Top panel: Schematic representation of the self-assembly of polymersomes and their functionalization with ssDNA. Middle panel: TEM micrographs and schematic representations of: (A) **Pol1** polymersomes, (B) conjugates of **Pol1** with ssDNA **a** (Pol1-**a**), and (C) conjugates of **Pol1** with ssDNA **c** (**Pol1-c**); (D) **Pol3** polymersomes, (E) conjugates of **Pol3** with ssDNA **a** (**Pol3-a**), and (F) conjugates of **Pol3** with ssDNA **c** (**Pol3-c**). Bottom panel: (G) Cryo-TEM micrograph of **Pol2**, (H) Schematic representation of a polymersome when its ssDNA is hybridized with the complementary ssDNA detection strand, and (I) normalized FCS autocorrelation curves (dots) together with the corresponding fit curves (lines) of: free Atto488 dye (20 nM, blue), **c**-Atto488 (20 nM, red), **Pol1-d** mixed with **c**-Atto488 (yellow), **Pol2-d** mixed with **c**-Atto488 (green), and **Pol3-d** mixed with **c**-Atto488 (purple).

S9D,E, Supporting Information). Brightness measurements allowed the number of ssDNA strands per polymersome to be quantified as 69 ± 9 for **Pol1-d**, 119 ± 24 for **Pol2-d**, and 88 ± 15 for **Pol3-d**. Similar values were obtained for polymersomes bearing **b** (Table S8, Supporting Information)**.** As expected, a higher density of azide groups available for coupling increases the number of ssDNA strands per polymersome (**Pol1-d** compared with **Pol2-d**), but for comparable azide surface densities (**Pol1** and **Pol3)**, there was no significant difference in the number of ssDNA strands per polymersome. This is likely the result of the lower surface curvature of **Pol3,** as electrostatic repulsion reduces DNA coverage density for less curved surfaces. [89].

Assembly and characterization of JNP-polymersome hybrid clusters

The inherent asymmetry of **JNP-II** and the asymmetric functionalization with ssDNA allow for highly specific self-organization between the Janus nanoparticles and polymersomes, using DNA hybridization as the driving force. Although the strength and specificity of DNA hybridization are well known, a critical aspect of the formation of JNP-polymersome clusters is the preservation of the integrity of the polymersomes. The relatively low ssDNA density on the polymersomes was selected to support attachment of polymersomes without affecting membrane integrity.

First, we evaluated mixtures of incompletely ssDNA-functionalized JNPs (**JNP-a**, or **JNP-c**) with complementary ssDNA-functionalized polymersomes. For both pairings, ssDNA-functionalized polymersomes attached to both lobes, and not just to the lobe exposing the complementary ssDNA strand, (Fig. S10A,B, Supporting Information). Similarly, unfunctionalized polymersomes adsorbed on both lobes of JNPs prior to ssDNA attachment (**JNP-II**) (Fig. S10C, Supporting Information). This non-specific adsorption indicates the presence of interactions between the polymersome membrane and the surface of either unfunctionalized JNP lobe. However, these interactions are shielded by ssDNA functionalization of the JNPs, and unfunctionalized polymersomes do not adhere to the completely

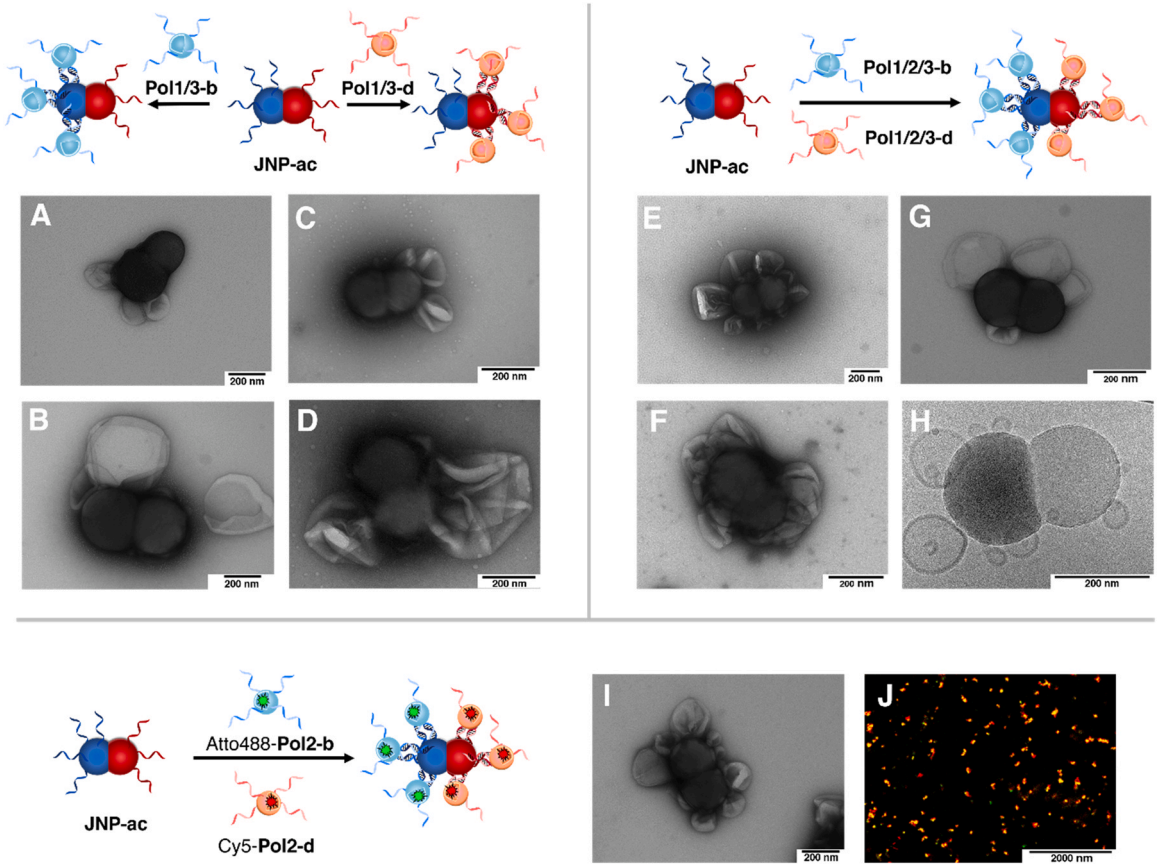

Fig. 4. Directional self-organization of JNPs and polymersomes mediated by DNA hybridization. Top left panel: Schematic representation of JNP-polymersome cluster when only one type of ssDNA-bearing polymersome is added, together with TEM micrographs of the polymersomes attached to the carboxylic acid-bearing lobe of **JNP-ac** after addition of (A) **Pol1-b** and (B) **Pol3-b**; and of polymersomes attached to the azide-bearing lobe of **JNP-ac** after addition of (C) **Pol1-d** and (D) **Pol3-d**. Top right panel: Schematic representation of JNP-polymersome cluster when both types of ssDNA-exposing polymersomes are simultaneously added, together with TEM micrographs of the clusters formed by mixing **JNP-ac** with (E) **Pol1-b** and **Pol1-d**, (F) **Pol2-b** and **Pol2-d**, (G) **Pol3-b** and **Pol3-d**. (H) Cryo-TEM micrographs of a cluster formed by mixing **JNP-ac** with **Pol1-b** and **Pol1-d**. Bottom panel: Schematic representation of JNP-polymersome cluster formation when combining **JNP-ac** with two types of ssDNA-exposing polymersomes loaded with cargo (Atto488-**Pol2-b** + Cy5-**Pol2-d**), together with the corresponding (I) TEM micrograph and (J) CLSM micrograph.

ssDNA-functionalized **JNP-ac** (Fig. S10D, Supporting Information). Therefore, full ssDNA functionalization of the JNP lobes is essential to preventing unspecific, non-DNA mediated interactions and to achieving the desired directionality of self-organization in JNPs-polymersome clusters.

Next, we combined doubly ssDNA-functionalized JNPs (**JNP-ac**) with one type of complementary, ssDNA-functionalized polymersome. Only the corresponding ssDNA functionalized-lobe was zipped with polymersomes, as evidenced by TEM (**JNP-ac** + **Pol1-b**, Fig. 4A; **JNP-ac** + **Pol3-b**, Fig. 4B; **JNP-ac** + **Pol1-d**, Fig. 4C; **JNP-ac** + **Pol3-d**, Fig. 4D), and the directionality was not affected by the size or ssDNA surface density of the polymersomes.

Finally, when **JNP-ac** was combined with mixtures of **b**- and **d**-bearing polymersomes, both JNP lobes were successfully zipped with polymersomes, as shown by TEM (**JNP-ac** + **Pol1-b + Pol1-d**, Fig. 4E and Fig. S11 A, B, Supporting Information, for additional overview TEM micrographs; **JNP-ac** + **Pol2-b + Pol2-d**, Fig. 4F; **JNP-ac** + **Pol3-b + Pol3-d**, Fig. 4G) and cryo-TEM (**JNP-ac** + **Pol1-b + Pol1-d**, Fig. 4H and Fig. S12, Supporting Information, for additional overview cryo-TEM images). By systematically changing the ratio of JNPs to polymersomes, as estimated by nanoparticle tracking analysis (NTA), we found 1:5:5 (**JNP-ac**:**Pol*i*-b:Pol*i*-d, *i* = 1–3**) to be the optimum ratio for the formation of JNP-polymersome clusters, and only few un-clustered components remained (Fig. S13, Supporting Information).

The average number of polymersomes attached to the JNP lobes was determined by analyzing the TEM micrographs of the clusters. These results showed that 3–4 "small" polymersomes (**Pol1** or **Pol2,** $R_h \approx 100$ nm) were bound to each lobe of **JNP-ac,** independent of the chemical nature of the lobe or the polymersome composition (Fig. 4A, C, E and Fig. S14A, Supporting Information). However, only ~2 polymersomes per lobe were bound to JNPs with the larger **Pol3** ($R_h \approx 200$ nm, Fig. 4B, D, F and Fig. S13B, Supporting Information). Since neither the ssDNA surface density on the JNP lobes nor on the polymersomes resulted in any difference, the overall composition of the clusters is essentially controlled by the size of the polymersomes within the parameter space explored here.

A unique advantage of combining "hard" and "soft" nano-objects is that JNPs provide a clear separation between orthogonal binding sites, while the polymersome membrane can both adapt to maximize the contact area and allows ssDNA strands to migrate to the site of adhesion. [61,90] This process enables a stronger and tighter contact between the components of the clusters than is possible between "hard" spheres. In addition, it permits the formation of clusters with a controlled upper size limit, which is not the case for DNA-mediated liposome cluster formation, for which aggregation has been observed. [32] However, the mobility of ssDNA strands within the membrane [61,91] results in a complex interplay of interactions compared to interactions among hard nanoparticles. [51] In polymersome-only clusters, the membranes are slightly deformed, flattening out in the contact region, [61,91] and this deformation is even higher with JNP-polymersome clusters (Fig. 4G). The physical stress that occurs when polymersomes attach to the JNPs is most pronounced near the edge of the adhesion zone, where

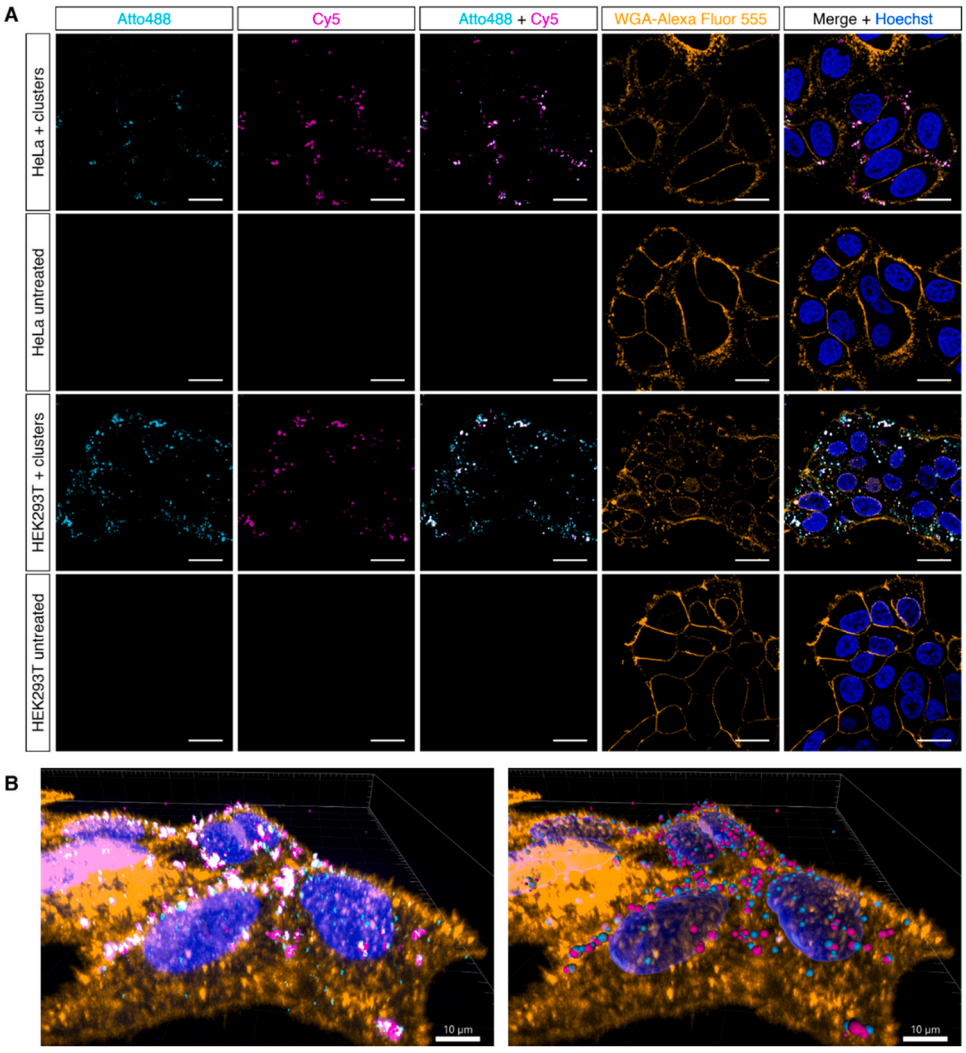

Fig. 5. Interaction of JNP-polymersome clusters with HeLa and HEK293T cells. (A) CLSM micrographs of HeLa and HEK293T cells after 24 h incubation with JNP-polymersome clusters. Atto488 channel: Atto488-**Pol2-b** (turquoise); Cy5 channel: Cy5-**Pol2-d** (magenta). The merged channel shows colocalization of both encapsulated dyes appearing in white, and additionally stained cell nuclei (Hoechst 33342, blue) and cell membranes (wheat germ agglutinin-Alexa Fluor 555, orange). Scale bars = 20 µm. (B) 3D projection of combined CLSM micrographs, showing accumulation of JNP-polymersome clusters on the surface of HeLa cells. Left: raw fluorescence of: cell nuclei (blue), cell membrane (orange), polymersomes Atto488-**Pol2-b** (turquoise) and Cy5-**Pol2-d** (magenta), colocalization of both visible in white. Right: fluorescence of polymersomes and cell nuclei reconstructed using IMARIS and raw fluorescence of cell membrane.

the membrane must make the transition from its natural curvature to relatively sharp angles in order to conform to the hard JNPs surface. However, the flexibility of the polymersome membrane based on PDMS-*b*-PMOXA enables cluster formation without membrane rupture.

To investigate the influence of the DNA zipping on the deformation of polymersomes upon cluster formation, we used ssDNA strands with different lengths. The length was increased by repeating the initial 22-nucleotide binding sequence from **a/b, c/d**, doubling (**a2/b2, c2/d2**) or quadrupling (**a4/b4, c4/d4**) the initial dsDNA linker length of ~7 nm [61] (Table S1 and S2). When ssDNA-functionalized JNPs (**JNP-a2c2** and **JNP-a4c4**) were combined with complementary ssDNA-bearing polymersomes (**Pol1-b2/Pol1-d2** and **Pol1-b4/Pol1-d4**, respectively), the clusters preserved the polymersome integrity and the average number of polymersomes per JNP lobe matched those observed for shorter strands (Table S4-S8, Fig. S15-S18, Supporting Information). As expected, an increase in DNA length induced a decrease in the adhesion area between polymersomes and JNPs, and reduced the membrane deformation (Table S9, Supporting Information). To establish a lower boundary for the number of ssDNA strands participating in the zipping process, we measured the polymersome-JNP adhesion areas from TEM micrographs (Table S9, Supporting Information). Calculating the JNP ssDNA surface density and assuming a uniform distribution of ssDNA on the JNP lobes, we estimated the number of ssDNA strands present in the adhesion area. Just ≤ 20% of polymersome ssDNA strands were involved in cluster formation (Table S10, Supporting Information), with more ssDNA strands per polymersome participating in binding to the acid lobe than to the azide lobe of JNPs (Table S9, Supporting Information). Thus, there is a significant fraction of ssDNA strands that are not involved in cluster formation and remain free for participation in further interactions, *e.g.* with cell receptors.

Loading of JNP-polymersome clusters and in vitro studies

With the aim of exploring possible applications of JNP-polymersome clusters, we loaded polymersomes with dyes as model molecules for low molecular weight cargo (*e.g.* drugs or contrast agents). Loading of different molecules in each polymersome type (**Poli-b and Poli-d, *i* = 1–3**) instead of co-encapsulation in one polymersome will both increase the encapsulation efficiency and

avoid inactivation/denaturation of sensitive molecules when located in the same compartment.

Doubly ssDNA-functionalized JNPs (**JNP-ac**) formed clusters when combined with two differently dye-loaded polymersomes (Atto488-**Pol2-b** and Cy5-**Pol2-d**) as indicated by TEM (Fig. 4I). The simultaneous and directed zipping of both dye-loaded polymersomes to the corresponding lobes of the JNPs was indicated by the colocalization of the fluorescent signals associated with the dyes in CLSM micrographs (Fig. 4J and Fig. S19-S20, Supporting Information). The dye-loaded polymersomes preserved their integrity upon cluster formation, as there was no fluorescent background associated with dye release (Fig. S20, Supporting Information). Then, we investigated the cell toxicity of the clusters using an MTS cell viability assay and observed no significant toxicity of the clusters or their components on HeLa cells up to concentrations of 40 $\mu g\,mL^{-1}$ (see Methods and Fig. S21 in the Supporting Information).

To understand how the clusters interact with the cells, we selected HeLa and HEK293T cell lines, as their expression of scavenger receptors and receptor-mediated interaction with DNA-functionalized carriers have been studied previously. [57,92] First, we investigated dye-loaded polymersomes without and with ssDNA functionalization (Atto488-**Pol2** and Atto488-**Pol2-d**, respectively). For both cell lines, only polymersomes with exposed ssDNA adhered to the cell membrane (Fig. S22, Supporting Information), consistent with previous reports. [57,92] JNP-polymersome clusters (**JNP-ac** + Atto488-**Pol2-b** + Cy5-**Pol2-d**) accumulated on the cell membranes of both cell lines, and colocalization of the fluorescence from the two polymersome-encapsulated dyes shows that the clusters preserved their architecture even in the complex extracellular environment (Fig. 5). Then, based on the hypothesis that scavenger receptors (SR) mediate the cluster-cell interaction, we used polyinosinic acid (PolyI) as a competitive SR inhibitor. A significant decrease in the accumulation of the JNP-polymersome clusters on HeLa cells was observed with increasing inhibitor concentration (0–50 $\mu g\,mL^{-1}$, Fig. S23, Supporting Information). At [PolyI] = 50 $\mu g\,mL^{-1}$, the clusters did not bind at all, indicating that SR plays a key role in the cluster-cell interaction. The difference in accumulation of clusters between HEK293T and HeLa cells might consequently result from differing levels of SR expression.

Conclusions

In summary, we have introduced a general strategy for the programmable production of hybrid “hard/soft” clusters comprised of dissimilar nanoassemblies and self-organized by DNA hybridization. These clusters with the directional organization of a molecular factory enable the simultaneous co-encapsulation of different molecules without affecting the properties or functionality of the cargo, due to controlled spatial segregation. “Hard” Janus nanoparticles with orthogonally addressable lobes enable directional interaction with “soft” polymersomes. By exploring different factors influencing the self-organization process, we have demonstrated that the final composition of the clusters is mainly controlled by the size of the polymersomes. Moreover, although the polymersome membrane is significantly deformed upon cluster formation, it remains intact due to its inherent flexibility and mechanical robustness. The clusters combine a number of properties key for applications in biomedicine: first, they preserve the constituent polymersomes’ integrity even in complex media, maintaining the encapsulation of enclosed cargo. Second, the clusters or their components are not cytotoxic and interact specifically with cells. Third, the JNP-polymersome hierarchical self-organization enables great compositional modularity as a key element for future biomedical applications. In combination, these favorable features predestines the JNP-polymersome clusters for sophisticated applications *e.g.* in correlative imaging, [18] as agents in nanotheranostics, [86] the co-delivery of pharmaceutically active species without the need of specifically developing combination formulations, [76,77,93] for enzymatic signaling cascades, [94] or for probing the extracellular matrix. [95].

Funding

This research is funded by the National Centre of Competence in Research - Molecular Systems Engineering (Project No. NCH1663), the Swiss National Science Foundation (Project No. 200020_172604) and the University of Basel.

Data Availability

Data will be made available on request.

Declaration of Competing Interest

The authors declare that they have no known competing financial interests or personal relationships that could have appeared to influence the work reported in this paper.

Acknowledgements

We gratefully acknowledge the National Centre of Competence in Research - Molecular Systems Engineering, the Swiss National Science Foundation and the University of Basel for funding. We thank Dr. R. Wehr for the synthesis of the copolymers, Dr. D. Wu for preliminary experiments in Janus nanoparticle synthesis and Dr. V. Maffeis, M. Muthwill for preliminary experiments on polymersome formation and functionalization. We thank Dr. M. Chami (BioEM Lab, C-CINA, Center for Cellular Imaging and NanoAnalytics, Biozentrum, University of Basel) for the Cryo-TEM micrographs. We are grateful to the late Prof. W. Meier for the support and discussions regarding the concept of this study and to Profs. E. Constable and B. Goodman for reading the manuscript.

CRediT authorship contribution statement

Conceptualization: C. G. Palivan, Methodology: V. Mihali, M. Skowicki, D. Messmer, Investigation: V. Mihali, M. Skowicki, Visualization: V. Mihali, M. Skowicki, D. Messmer, Funding acquisition: C. G. Palivan, Writing – original draft: V. Mihali, M. Skowicki, D. Messmer, C. G. Palivan, Writing – review & editing: V. Mihali, M. Skowicki, D. Messmer, C. G. Palivan.

Appendix A. Supporting information

Supplementary data associated with this article can be found in the online version at doi:10.1016/j.nantod.2022.101741.

References

[1] E. Karsenti, Self-organization in cell biology: a brief history, Nat. Rev. Mol. Cell Biol. 9 (3) (2008) 255–262, https://doi.org/10.1038/nrm2357
[2] W. Pfeifer, B. Saccà, From nano to macro through hierarchical self-assembly: the dna paradigm, ChemBioChem 17 (12) (2016) 1063–1080, https://doi.org/10.1002/cbic.201600034
[3] S. Zhang, C.I. Pelligra, X. Feng, C.O. Osuji, Directed assembly of hybrid nanomaterials and nanocomposites, Adv. Mater. 30 (18) (2018) 1705794, https://doi.org/10.1002/adma.201705794
[4] I. Cobo, M. Li, B.S. Sumerlin, S. Perrier, Smart hybrid materials by conjugation of responsive polymers to biomacromolecules, Nat. Mater. 14 (2) (2014) 143–159, https://doi.org/10.1038/nmat4106
[5] C. Sanchez, H. Arribart, M.M.G. Guille, Biomimetism and bioinspiration as tools for the design of innovative materials and systems, Nat. Mater. 4 (4) (2005) 277–288, https://doi.org/10.1038/nmat1339
[6] A. Wang, J. Huang, Y. Yan, Hierarchical molecular self-assemblies: construction and advantages, Soft Matter 10 (19) (2014) 3362–3373, https://doi.org/10.1039/c3sm53214c

[7] C. Gong, S. Sun, Y. Zhang, L. Sun, Z. Su, A. Wu, G. Wei, Hierarchical nanomaterials via biomolecular self-assembly and bioinspiration for energy and environmental applications, Nanoscale 11 (10) (2019) 4147–4182, https://doi.org/10.1039/c9nr00218a

[8] J. Kong, W. Li, S. Zhao, J. Zhang, T. Yue, Y. Wang, Y. Xia, Z. Li, J. Kong, W. Li, S. Zhao, T. Yue, Y. Xia, Z. Li, J. Zhang, Y. Wang, Color-tunable fluorescent hierarchical nanoassemblies with concentration-encoded emission, Small 18 (27) (2022) 2201826, https://doi.org/10.1002/smll.202201826

[9] R.M. Kramer, W.J. Crookes-Goodson, R.R. Naik, The self-organizing properties of squid reflectin protein, Nat. Mater. 6 (7) (2007) 533–538, https://doi.org/10.1038/nmat1930

[10] L. Liang, P. Zheng, C. Zhang, I. Barman, A programmable DNA-silicification-based nanocavity for single-molecule plasmonic sensing, Adv. Mater. 33 (7) (2021) 2005133, https://doi.org/10.1002/adma.202005133

[11] M.P. Zhuo, J.J. Wu, X.D. Wang, Y.C. Tao, Y. Yuan, L.S. Liao, Hierarchical self-assembly of organic heterostructure nanowires, Nat. Commun. 10 (2019) 3839, https://doi.org/10.1038/s41467-019-11731-7

[12] Y. Gao, J. Zhao, Z. Huang, T.K. Ronson, F. Zhao, Y. Wang, B. Li, C. Feng, Y. Yu, Y. Cheng, D. Yang, X.J. Yang, B. Wu, Hierarchical self-assembly of adhesive and conductive gels with anion-coordinated triple helicate junctions, Angew. Chem. Int. Ed. 61 (22) (2022) e202201793, https://doi.org/10.1002/anie.202201793

[13] Y. Wang, L. Sun, C. Wang, F. Yang, X. Ren, X. Zhang, H. Dong, W. Hu, Organic crystalline materials in flexible electronics, Chem. Soc. Rev. 48 (6) (2019) 1492–1530, https://doi.org/10.1039/c8cs00406d

[14] A.M. Wen, N.F. Steinmetz, Design of virus-based nanomaterials for medicine, biotechnology, and energy, Chem. Soc. Rev. 45 (15) (2016) 4074–4126, https://doi.org/10.1039/c5cs00287g

[15] J.K. Pokorski, N.F. Steinmetz, The art of engineering viral nanoparticles, Mol. Pharm. 8 (1) (2011) 29–43, https://doi.org/10.1021/mp100225y

[16] X. Zhang, C. Gong, O.U. Akakuru, Z. Su, A. Wu, G. Wei, The design and biomedical applications of self-assembled two-dimensional organic biomaterials, Chem. Soc. Rev. 48 (23) (2019) 5564–5595, https://doi.org/10.1039/c8cs01003j

[17] Z. Zhao, J.C.Y. Wang, M. Zhang, N.A. Lyktey, M.F. Jarrold, S.C. Jacobson, A. Zlotnick, Asymmetrizing an icosahedral virus capsid by hierarchical assembly of subunits with designed asymmetry, Nat. Commun. 12 (2021) 589, https://doi.org/10.1038/s41467-020-20862-1

[18] A. Walter, P. Paul-Gilloteaux, B. Plochberger, L. Sefc, P. Verkade, J.G. Mannheim, P. Slezak, A. Unterhuber, M. Marchetti-Deschmann, M. Ogris, K. Bühler, D. Fixler, S.H. Geyer, W.J. Weninger, M. Glösmann, S. Handschuh, T. Wanek, Correlated multimodal imaging in life sciences: expanding the biomedical horizon, Front. Phys. 8 (2020) 47, https://doi.org/10.3389/fphy.2020.00047

[19] C. Sanchez, K.J. Shea, S. Kitagawa, L. Lur´s, D. Carlos, R.A.S. Ferreira, Z. Bermudez, B.J. Julia´n-Lo´pezlo´pez, P.P. Escribano, Progress on lanthanide-based organic–inorganic hybrid phosphors, Chem. Soc. Rev. 40 (2) (2011) 536–549, https://doi.org/10.1039/c0cs00069h

[20] S.S. Kelkar, T.M. Reineke, Theranostics: combining imaging and therapy, Biconjug. Chem. 22 (10) (2011) 1879–1903, https://doi.org/10.1021/bc200151q

[21] J. Zhang, L. Ning, J. Huang, C. Zhang, K. Pu, Activatable molecular agents for cancer theranostics, Chem. Sci. 11 (3) (2020) 618–630, https://doi.org/10.1039/c9sc05460j

[22] S. Gadde, Multi-drug delivery nanocarriers for combination therapy, Med. Chem. Commun. 6 (11) (2015) 1916–1929, https://doi.org/10.1039/c5md00365b

[23] Z. Yang, D. Gao, Z. Cao, C. Zhang, D. Cheng, J. Liu, X. Shuai, Drug and gene co-delivery systems for cancer treatment, Biomater. Sci. 3 (7) (2015) 1035–1049, https://doi.org/10.1039/c4bm00369a

[24] P. Ray, N. Haideri, Haquem Inamul, O. Mohammed, S. Chakraborty, S. Banerjee, M. Quadir, A.E. Brinker, S.K. Banerjee, The impact of nanoparticles on the immune system: a gray zone of nanomedicine, J. Immunol. Sci. 5 (1) (2021) 19–33, https://doi.org/10.29245/2578-3009/2021/1.1206

[25] T.M. Allen, P.R. Cullis, Liposomal drug delivery systems: from concept to clinical applications, Adv. Drug Deliv. Rev. 65 (1) (2013) 36–48, https://doi.org/10.1016/j.addr.2012.09.037

[26] C.G. Palivan, R. Goers, A. Najer, X. Zhang, A. Car, W. Meier, Bioinspired polymer vesicles and membranes for biological and medical applications, Chem. Soc. Rev. 45 (2) (2016) 377–411, https://doi.org/10.1039/C5CS00569H

[27] M. Shimomura, T. Sawadaishi, Bottom-up strategy of materials fabrication: a new trend in nanotechnology of soft materials, Curr. Opin. Colloid Interface Sci. 6 (1) (2001) 11–16, https://doi.org/10.1016/s1359-0294(00)00081-9

[28] K.C. Tjandra, C.R. Forest, C.K. Wong, S. Alcantara, H.G. Kelly, Y. Ju, M.H. Stenzel, J.A. McCarroll, M. Kavallaris, F. Caruso, S.J. Kent, P. Thordarson, Modulating the selectivity and stealth properties of ellipsoidal polymersomes through a multivalent peptide ligand display, Adv. Healthc. Mater. 9 (13) (2020) 2000261, https://doi.org/10.1002/adhm.202000261

[29] J. Li, Y. Anraku, K. Kataoka, Self-boosting catalytic nanoreactors integrated with triggerable crosslinking membrane networks for initiation of immunogenic cell death by pyroptosis, Angew. Chem. 132 (32) (2020) 13628–13632, https://doi.org/10.1002/ange.202004180

[30] Y. Fukushima, S. Uchida, H. Imai, H. Nakatomi, K. Kataoka, N. Saito, K. Itaka, Treatment of ischemic neuronal death by introducing brain-derived neurotrophic factor MRNA using polyplex nanomicelle, Biomaterials 270 (2021) 120681, https://doi.org/10.1016/j.biomaterials.2021.120681

[31] J. Leong, Y. Teo, V.K. Aakalu, Y.Y. Yang, H. Kong, J. Leong, J.Y. Teo, Y.Y. Yang, V.K. Aakalu, H. Kong, Engineering polymersomes for diagnostics and therapy, Adv. Healthc. Mater. 7 (8) (2018) 1701276, https://doi.org/10.1002/adhm.201701276

[32] G. Stengel, R. Zahn, F. Höök, DNA-induced programmable fusion of phospholipid vesicles, J. Am. Chem. Soc. 129 (31) (2007) 9584–9585, https://doi.org/10.1021/ja073200k

[33] C. Yang, Z.I. Lin, J.A. Chen, Z. Xu, J. Gu, W.C. Law, J.H.C. Yang, C.K. Chen, Organic/inorganic self-assembled hybrid nano-architectures for cancer therapy applications, Macromol. Biosci. 22 (2) (2022) 2100349, https://doi.org/10.1002/mabi.202100349

[34] B. Niu, Y. Chen, L. Zhang, J. Tan, Organic–inorganic hybrid nanomaterials prepared via polymerization-induced self-assembly: recent developments and future opportunities, Polym. Chem. 13 (18) (2022) 2554–2569, https://doi.org/10.1039/d2py00180b

[35] S. Mann, Self-assembly and transformation of hybrid nano-objects and nanostructures under equilibrium and non-equilibrium conditions, Nat. Mater. 8 (10) (2009) 781–792, https://doi.org/10.1038/nmat2496

[36] M. Li, E. Dujardin, S. Mann, Programmed assembly of multi-layered protein/nanoparticle-carbon nanotube conjugates, Chem. Commun. (No. 39) (2005) 4952–4954, https://doi.org/10.1039/b509109h

[37] D. Gottlieb, S.A. Morin, S. Jin, R.T. Raines, Self-assembled collagen-like peptide fibers as templates for metallic nanowires, J. Mater. Chem. 18 (32) (2008) 3865–3870, https://doi.org/10.1039/b807150k

[38] H. Wang, W. Lin, K.P. Fritz, G.D. Scholes, M.A. Winnik, I. Manners, Cylindrical block co-micelles with spatially selective functionalization by nanoparticles, J. Am. Chem. Soc. 129 (43) (2007) 12924–12925, https://doi.org/10.1021/ja075587x

[39] F. Jia, Y. Zhang, B. Narasimhan, S.K. Mallapragada, Block copolymer-quantum dot micelles for multienzyme colocalization, Langmuir 28 (50) (2012) 17389–17395, https://doi.org/10.1021/la303115t

[40] E. Amstad, J. Kohlbrecher, E. Müller, T. Schweizer, M. Textor, E. Reimhult, Triggered release from liposomes through magnetic actuation of iron oxide nanoparticle containing membranes, Nano Lett. 11 (4) (2011) 1664–1670, https://doi.org/10.1021/nl2001499

[41] E. Amstad, S.H. Kim, D.A. Weitz, Photo- and thermoresponsive polymersomes for triggered release, Angew. Chem. Int. Ed. 51 (50) (2012) 12499–12503, https://doi.org/10.1002/anie.201206531

[42] B. Iyisan, A. Janke, P. Reichenbach, L.M. Eng, D. Appelhans, B. Voit, Immobilized multifunctional polymersomes on solid surfaces: infrared light-induced selective photochemical reactions, PH responsive behavior, and probing mechanical properties under liquid phase, ACS Appl. Mater. Interfaces 8 (24) (2016) 15788–15801, https://doi.org/10.1021/acsami.6b03525

[43] S. Rigo, G. Gunkel-Grabole, W. Meier, C.G. Palivan, Surfaces with dual functionality through specific coimmobilization of self-assembled polymeric nanostructures, Langmuir 35 (13) (2019) 4557–4565, https://doi.org/10.1021/acs.langmuir.8b02812

[44] Y. Cui, H. Zhu, J. Cai, H. Qiu, Self-regulated Co-assembly of soft and hard nanoparticles, Nat. Commun. 12 (2021) 5682, https://doi.org/10.1038/s41467-021-25995-5

[45] A. Sánchez, K. Ovejero Paredes, J. Ruiz-Cabello, P. Martínez-Ruíz, J.M. Pingarrón, R. Villalonga, M. Filice, Hybrid decorated core@shell Janus nanoparticles as a flexible platform for targeted multimodal molecular bioimaging of cancer, ACS Appl. Mater. Interfaces 10 (37) (2018) 31032–31043, https://doi.org/10.1021/acsami.8b10452

[46] X. Fan, J. Yang, J. Loh, Z. Li, X. Fan, J. Yang, X.J. Loh, Z. Li, Polymeric Janus nanoparticles: recent advances in synthetic strategies, materials properties, and applications, Macromol. Rapid Commun. 40 (5) (2019) 1800203, https://doi.org/10.1002/marc.201800203

[47] V. Mihali, A. Honciuc, Self-assembly of strongly amphiphilic Janus nanoparticles into freestanding membranes, Adv. Mater. Interfaces 9 (4) (2022) 2101713, https://doi.org/10.1002/admi.202101713

[48] C. Kang, A. Honciuc, Self-assembly of Janus nanoparticles into transformable suprastructures, J. Phys. Chem. Lett. 9 (6) (2018) 1415–1421, https://doi.org/10.1021/acs.jpclett.8b00206

[49] C. Kang, A. Honciuc, Versatile triblock Janus nanoparticles: synthesis and self-assembly, Chem. Mater. 31 (5) (2019) 1688–1695, https://doi.org/10.1021/acs.chemmater.8b05073

[50] A. Walther, A.H.E. Müller, Janus particles: synthesis, self-assembly, physical properties, and applications, Chem. Rev. 113 (7) (2013) 5194–5261, https://doi.org/10.1021/cr300089t

[51] H. Xing, Z. Wang, Z. Xu, N.Y. Wong, Y. Xiang, G.L. Liu, Y. Lu, DNA-directed assembly of asymmetric nanoclusters using Janus nanoparticles, ACS Nano 6 (1) (2012) 802–809, https://doi.org/10.1021/nn2042797

[52] M. Marguet, C. Bonduelle, S. Lecommandoux, Multicompartmentalized polymeric systems: towards biomimetic cellular structure and function, Chem. Soc. Rev. 42 (2) (2012) 512–529, https://doi.org/10.1039/c2cs35312a

[53] A. Küchler, M. Yoshimoto, S. Luginbühl, F. Mavelli, P. Walde, Enzymatic reactions in confined environments, Nat. Nanotechnol. 11 (5) (2016) 409–420, https://doi.org/10.1038/nnano.2016.54

[54] A. Belluati, I. Craciun, C.E. Meyer, S. Rigo, C.G. Palivan, Enzymatic reactions in polymeric compartments: nanotechnology meets nature, Curr. Opin. Biotechnol. 60 (2019) 53–62, https://doi.org/10.1016/j.copbio.2018.12.011

[55] F. Itel, A. Najer, C.G. Palivan, W. Meier, Dynamics of membrane proteins within synthetic polymer membranes with large hydrophobic mismatch, Nano Lett. 15 (6) (2015) 3871–3878, https://doi.org/10.1021/acs.nanolett.5b00699

[56] E. Rideau, R. Dimova, P. Schwille, F.R. Wurm, K. Landfester, Liposomes and polymersomes: a comparative review towards cell mimicking, Chem. Soc. Rev. 47 (23) (2018) 8572–8610, https://doi.org/10.1039/c8cs00162f

[57] J. Liu, I. Craciun, A. Belluati, D. Wu, S. Sieber, T. Einfalt, D. Witzigmann, M. Chami, J. Huwyler, C.G. Palivan, DNA-directed arrangement of soft synthetic compartments and their behavior in vitro and in vivo, Nanoscale 12 (17) (2020) 9786–9799, https://doi.org/10.1039/d0nr00361a
[58] D.E. Discher, A. Eisenberg, Polymer vesicles, Science 297 (5583) (2002) 967–973, https://doi.org/10.1126/science.1074972
[59] J.F. Le Meins, O. Sandre, S. Lecommandoux, Recent trends in the tuning of polymersomes' membrane properties, Eur. Phys. J. E 34 (2011) 14, https://doi.org/10.1140/epje/i2011-11014-y
[60] T. Einfalt, D. Witzigmann, C. Edlinger, S. Sieber, R. Goers, A. Najer, M. Spulber, O. Onaca-Fischer, J. Huwyler, C.G. Palivan, Biomimetic artificial organelles with in vitro and in vivo activity triggered by reduction in microenvironment, Nat. Commun. 9 (2018) 1127, https://doi.org/10.1038/s41467-018-03560-x
[61] J. Liu, V. Postupalenko, S. Lörcher, D. Wu, M. Chami, W. Meier, C.G. Palivan, DNA-mediated self-organization of polymeric nanocompartments leads to interconnected artificial organelles, Nano Lett. 16 (11) (2016) 7128–7136, https://doi.org/10.1021/acs.nanolett.6b03430
[62] V. Maffeis, A. Belluati, I. Craciun, D. Wu, S. Novak, C.-A. Schoenenberger, C.G. Palivan, Clustering of catalytic nanocompartments for enhancing an extracellular non-native cascade reaction, Chem. Sci. 12 (2021) 12274–12285, https://doi.org/10.1039/d1sc04267j
[63] T. Kamperman, M. Koerselman, C. Kelder, J. Hendriks, J.F. Crispim, X. de Peuter, P.J. Dijkstra, M. Karperien, J. Leijten, Spatiotemporal material functionalization via competitive supramolecular complexation of avidin and biotin analogs, Nat. Commun. 10 (2019) 4347, https://doi.org/10.1038/s41467-019-12390-4
[64] N.C. Seeman, Nanomaterials based on DNA, Annu. Rev. Biochem. 79 (2010) 65–87, https://doi.org/10.1146/annurev-biochem-060308-102244
[65] A.V. Pinheiro, D. Han, W.M. Shih, H. Yan, Challenges and opportunities for structural DNA nanotechnology, Nat. Nanotechnol. 6 (12) (2011) 763–772, https://doi.org/10.1038/nnano.2011.187
[66] X. Liu, C.H. Lu, I. Willner, Switchable reconfiguration of nucleic acid nanostructures by stimuli-responsive DNA machines, Acc. Chem. Res. 47 (6) (2014) 1673–1680, https://doi.org/10.1021/ar400316h
[67] P.Y. W Dankers, T.M. Hermans, T.W. Baughman, Y. Kamikawa, R.E. Kieltyka, M.M. C Bastings, H.M. Janssen, N.A. J M Sommerdijk, A. Larsen, M.J. A van Luyn, A.W. Bosman, E.R. Popa, G. Fytas, E.W. Meijer, P.Y. W Dankers, T.M. Hermans, R.E. Kieltyka, M.M. C Bastings, M.J. A van Luyn, E.R. Popa, T.W. Baughman, Y. Kamikawa, H.M. Janssen, N.A. J M Sommerdijk, A. Larsen, G. Fytas, A.W. Bosman, Hierarchical formation of supramolecular transient networks in water: a modular injectable delivery system, Adv. Mater. 24 (20) (2012) 2703–2709, https://doi.org/10.1002/adma.201104072
[68] A.H. Gröschel, A. Walther, T.I. Löbling, F.H. Schacher, H. Schmalz, A.H.E. Müller, Guided hierarchical Co-assembly of soft patchy nanoparticles, Nature 503 (7475) (2013) 247–251, https://doi.org/10.1038/nature12610
[69] K. Keren, R.S. Berman, E. Buchstab, U. Sivan, E. Braun, DNA-templated carbon nanotube field-effect transistor, Science 302 (5649) (2003) 1380–1382 https://doi.org/110.1126/science.1091022.
[70] M.R. Jones, N.C. Seeman, C.A. Mirkin, Programmable materials and the nature of the DNA bond, Science 347 (2015) 1260901, https://doi.org/10.1126/science.1260901
[71] L. Cademartiri, K.J.M. Bishop, Programmable self-assembly, Nat. Mater. 14 (1) (2014) 2–9, https://doi.org/10.1038/nmat4184
[72] A.M. Hung, C.M. Micheel, L.D. Bozano, L.W. Osterbur, G.M. Wallraff, J.N. Cha, Large-area spatially ordered arrays of gold nanoparticles directed by lithographically confined DNA origami, Nat. Nanotechnol. 5 (2) (2009) 121–126, https://doi.org/10.1038/nnano.2009.450
[73] R.J. Macfarlane, B. Lee, M.R. Jones, N. Harris, G.C. Schatz, C.A. Mirkin, Nanoparticle superlattice engineering with DNA, Science 334 (6053) (2011) 204–208, https://doi.org/10.1126/science.1210493
[74] C.A. Mirkin, R.L. Letsinger, R.C. Mucic, J.J. Storhoff, A DNA-based method for rationally assembling nanoparticles into macroscopic materials, Nature 382 (6592) (1996) 607–609, https://doi.org/10.1038/382607a0
[75] A.P. Alivisatos, K.P. Johnsson, X. Peng, T.E. Wilson, C.J. Loweth, M.P. Bruchez, P.G. Schultz, Organization of "nanocrystal Molecules" Using DNA, Nature 382 (6592) (1996) 609–611, https://doi.org/10.1038/382609a0
[76] S.S. Qi, J.H. Sun, H.H. Yu, S.Q. Yu, Co-delivery nanoparticles of anti-cancer drugs for improving chemotherapy efficacy, Drug Deliv. 24 (1) (2017) 1909–1926, https://doi.org/10.1080/10717544.2017.1410256
[77] S. Lv, Z. Tang, M. Li, J. Lin, W. Song, H. Liu, Y. Huang, Y. Zhang, X. Chen, Co-delivery of doxorubicin and paclitaxel by PEG-polypeptide nanovehicle for the treatment of non-small cell lung cancer, Biomaterials 35 (23) (2014) 6118–6129, https://doi.org/10.1016/j.biomaterials.2014.04.034
[78] Y. Li, Y. Jiang, Z. Zheng, N. Du, S. Guan, W. Guo, X. Tang, J. Cui, L. Zhang, K. Liu, Q. Yu, Z. Gan, Y.Q. Li, Y.T. Jiang, Z.Y. Zheng, N. Du, S.L. Guan, W.X. Guo, X.H. Tang, J.J.Z. Cui, L.Q. Zhang, K.P. Liu, Q.S. Yu, Z.H. Gan, Co-delivery of precisely prescribed multi-prodrug combination by an engineered nanocarrier enables efficient individualized cancer chemotherapy, Adv. Mater. 34 (12) (2022) 2110490, https://doi.org/10.1002/adma.202110490
[79] D.D. Zhang, Y.Y. Kong, J.H. Sun, S.J. Huo, M. Zhou, Y.L. Gui, X. Mu, H. Chen, S.Q. Yu, Q. Xu, Co-delivery nanoparticles with characteristics of intracellular precision release drugs for overcoming multidrug resistance, Int. J. Nanomed. 12 (2017) 2081–2108, https://doi.org/10.2147/ijn.s128790
[80] S.C. Shetty, N. Yandrapalli, K. Pinkwart, D. Krafft, T. Vidakovic-Koch, I. Ivanov, T. Robinson, Directed signaling cascades in monodisperse artificial eukaryotic cells, ACS Nano 15 (10) (2021) 15656–15666, https://doi.org/10.1021/acsnano.1c04219
[81] S. Thamboo, A. Najer, A. Belluati, C. Planta, D. von; Wu, I. Craciun, W. Meier, C.G. Palivan, Mimicking cellular signaling pathways within synthetic multicompartment vesicles with triggered enzyme activity and induced ion channel recruitment, Adv. Funct. Mater. 29 (40) (2019) 1904267, https://doi.org/10.1002/adfm.201904267
[82] A. Belluati, S. Thamboo, A. Najer, V. Maffeis, C. Planta, I. Craciun, C.G. Palivan, W. Meier, Multicompartment polymer vesicles with artificial organelles for signal-triggered cascade reactions including cytoskeleton formation, Adv. Funct. Mater. 30 (32) (2020) 2002949, https://doi.org/10.1002/adfm.202002949
[83] E.B. Mock, H. De Bruyn, B.S. Hawkett, R.G. Gilbert, C.F. Zukoski, Synthesis of anisotropic nanoparticles by seeded emulsion polymerization, Langmuir 22 (9) (2006) 4037–4043, https://doi.org/10.1021/la060003a
[84] D. Bartczak, A.G. Kanaras, Preparation of peptide-functionalized gold nanoparticles using one pot EDC/Sulfo-NHS coupling, Langmuir 27 (16) (2011) 10119–10123, https://doi.org/10.1021/la2022177
[85] E. Kim, H. Koo, Biomedical applications of copper-free click chemistry: in vitro, in vivo, and ex vivo, Chem. Sci. 10 (34) (2019) 7835–7851, https://doi.org/10.1039/c9sc03368h
[86] C.E. Meyer, J. Liu, I. Craciun, D. Wu, H. Wang, M. Xie, M. Fussenegger, C.G. Palivan, Segregated nanocompartments containing therapeutic enzymes and imaging compounds within DNA-zipped polymersome clusters for advanced nanotheranostic platform, Small 16 (27) (2020) 1906492, https://doi.org/10.1002/smll.201906492
[87] C. Lopresti, M. Massignani, C. Fernyhough, A. Blanazs, A.J. Ryan, J. Madsen, N.J. Warren, S.P. Armes, A.L. Lewis, S. Chirasatitsin, A.J. Engler, G. Battaglia, Controlling polymersome surface topology at the nanoscale by membrane confined polymer/polymer phase separation, ACS Nano 5 (3) (2011) 1775–1784, https://doi.org/10.1021/nn102455z
[88] W. Burchard, Static and dynamic light scattering from branched polymers and biopolymers, Advances in Polymer Science, Springer, Berlin, Heidelberg, 1983, pp. 1–124, https://doi.org/10.1007/3-540-12030-0_1
[89] A. Kira, H. Kim, K. Yasuda, Contribution of nanoscale curvature to number density of immobilized DNA on gold nanoparticles, Langmuir 25 (3) (2009) 1285–1288, https://doi.org/10.1021/la803385x
[90] L. Parolini, B.M. Mognetti, J. Kotar, E. Eiser, P. Cicuta, L. Di Michele, Volume and porosity thermal regulation in lipid mesophases by coupling mobile ligands to soft membranes, Nat. Commun. 6 (2015) 5948, https://doi.org/10.1038/ncomms6948
[91] R. Luo, K. Göpfrich, I. Platzman, J.P. Spatz, DNA-based assembly of multi-compartment polymersome networks, Adv. Funct. Mater. 30 (46) (2020) 2003480, https://doi.org/10.1002/adfm.202003480
[92] P.C. Patel, D.A. Giljohann, W.L. Daniel, D. Zheng, A.E. Prigodich, C.A. Mirkin, Scavenger receptors mediate cellular uptake of polyvalent oligonucleotide-functionalized gold nanoparticles, Bioconjug. Chem. 21 (12) (2010) 2250–2256, https://doi.org/10.1021/bc1002423
[93] S. Guo, C.M. Lin, Z. Xu, L. Miao, Y. Wang, L. Huang, Co-delivery of cisplatin and rapamycin for enhanced anticancer therapy through synergistic effects and microenvironment modulation, ACS Nano 8 (5) (2014) 4996–5009, https://doi.org/10.1021/nn5010815
[94] R. Siedentop, C. Claaßen, D. Rother, S. Lütz, K. Rosenthal, Getting the most out of enzyme cascades: strategies to optimize in vitro multi-enzymatic reactions, Catalysts 11 (10) (2021) 1183, https://doi.org/10.3390/catal11101183
[95] D.A.C. Walma, K.M. Yamada, The extracellular matrix in development, dev175596, Development 147 (10) (2020), https://doi.org/10.1242/dev.175596/224217